Determining the mechanical properties of small volumes of material from submicrometer spherical indentations

J. S. Field and M. V. Swain
Department of Mechanical Engineering, University of Sydney, New South Wales, 2006, Australia, and CSIRO Division of Applied Physics, Lindfield, New South Wales, 2070, Australia

(Received 30 December 1993; accepted 24 August 1994)

The stress/strain behavior of bulk material is usually investigated in uniaxial tension or compression; however, these methods are not generally available for very small volumes of material. Submicrometer indentation using a spherical indenter has the potential for filling this gap with, possibly, access to hardness and elastic modulus profiles, representative stress/strain curves, and the strain hardening index. The proposed techniques are based on principles well established in hardness testing using spherical indenters, but not previously applied to depth-sensing instruments capable of measurements on a submicrometer scale. These approaches are now adapted to the analysis of data obtained by stepwise indentation with partial unloading, a technique that facilitates separation of the elastic and plastic components of indentation at each step and is able to take account of the usually ignored phenomena of "piling up" and "sinking in".

I. INTRODUCTION

Indentation with a steel ball, introduced by Brinell[1] early this century to provide a means of quantifying the different qualities of iron and steel, engendered considerable interest at the time due to its ability to allow a number of materials properties to be investigated through a simple test. This ability arose from the strain hardening behavior of elastic/plastic materials and a simple relationship that exists between strain and the size of spherical indentations. Due to the ease with which stress strain curves can be obtained in uniaxial tension or compression, the use of spherical indentation for this purpose has been largely ignored and its use limited to bulk hardness testing in a form that minimizes the effects of strain variation. Limited in this way, the Brinell hardness test is not free of problems, among which are dependence of hardness number on test conditions, the large size of indentations that is unacceptable in precision engineering, and deformation of the steel balls used as indenters. This latter limits its application to soft materials. The Vickers, Knoop, and Rockwell tests, which use small diamond pyramids or cones, were introduced to avoid these problems and have become industry standards. The two former tests have also been used at very low loads to measure the nominal hardness of thin films or small volumes of materials. More recently, instrumented micromechanical probe systems using Berkovich indenters have been developed that enable the nominal hardness and modulus of localized volumes or thin films to be investigated.

Unfortunately, uniaxial tension or compression testing is not readily accessible to the developing field of surface engineering where the properties of thin surface layers and small volumes of individual material phases are of great importance. This need may be addressed by use of spherical indentation using small, very precise, diamond spherocones, as recently proposed by the authors.[2] Such an approach coupled with submicrometer penetration, stepwise loading, and measurement of penetration depth can be used to investigate hardness (or mean contact pressure) and elastic modulus as functions of penetration, produce representative stress/strain curves, and investigate strain hardening. It is the principal purpose of this paper to show that it is also possible, under suitable conditions, to take into account "piling up" or "sinking in" of the perimeter of indenter contact which is usually ignored, possibly leading to substantial error.

This paper is divided into two parts. In Sec. II the theoretical basis of spherical indentation is reviewed, with particular attention to piling up and sinking in. Also, available methods for analyzing data obtained from stepwise submicrometer indentation will be discussed. In the remainder, results of spherical indentation experiments, using submicrometer spherical indentation with partial unloading, will be examined in light of the theoretical arguments.

II. THEORY

A. General theoretical principles

Essential elements of the test proposed by Brinell[1] are the impression of a hard steel ball of diameter D into the surface of a test material with sufficient force P to produce a residual indentation with diameter $2a$ at the

surface and a depth of penetration d below the circle of contact, such that d/D is in the range 0.1 to 0.3. Over this range, indentation of metals is well behaved, and several experimentally observed relationships are found to hold.

The circle delimiting contact between the indenter and the indentation is not usually in the plane of the original surface but may be above or below it. This piling up or sinking in arises from distortion of the surface by material displaced by indentation and is controlled by the strain hardening properties of the material. The geometry of a loaded indentation with the circle of contact above the original surface (left), and below the original surface (right), is illustrated in Fig. 1.

Francis[3] argued that spherical indentation in elastic/plastic materials evolves in three distinct stages. In the first stage, while $P_m/Y < 1.1$, deformation is wholly elastic and follows the well-known Hertz law[4]; here P_m is the mean pressure over the projected contact area of the indentation and Y is the flow stress of the undeformed material. When P_m/Y reaches 1.1, a nucleus of plasticity forms at a point below the center of the region of contact. This occurs at a depth dependent on the strain hardening characteristics of the material but always close to $0.5a$. In materials susceptible to strain hardening the flow stress increases with increasing deformation and Y_ϵ represents flow stress at the level of strain ϵ, which has accumulated to this point. When $P_m/Y_\epsilon \approx 3.0$ full plastic flow is established and from this point on P_m/Y_ϵ remains approximately constant with P_m increasing only as necessary to accommodate an increase in Y_ϵ.

Johnson[5] correlated indentation data from a variety of sources and showed that during the transition from elastic deformation to full plastic flow, P_m/Y_ϵ can be represented as a logarithmic function of nondimensional strain $2E^*a/YD$ in which E^* is defined by

$$1/E^* = (1 - \nu_m^2)/E_m + (1 - \nu_i^2)/E_i \qquad (1)$$

In this expression ν_m and E_m are Poisson's ratio and Young's modulus for the indented material and ν_i and E_i are Poisson's ratio and Young's modulus for the indenter material, respectively. The transition to full plastic flow was shown to occur when $2E^*a/YD$ reaches approximately 30 in spherical indentation.

In Johnson's[5] expression for nondimensional strain, $2a/D$ is related to Tabor's[6] approximation for strain at the periphery of an indentation, namely

$$\epsilon_r = 0.4a/D \qquad (2)$$

During the development of full plastic flow, deformation at the surface is controlled by elastic mechanisms, and subsurface plastic flow is accommodated internally by elastic deformation of the surrounding material. The development of full plastic flow is quite rapid and is normally complete by the time a/D reaches 0.1, the lower limit of the so-called Meyer regime (see Tabor[6]). The upper limit of the Meyer regime may be extended to the geometric limit $a/D = 0.5$ without observable loss of reproducibility.

Strain in spherical indentation is maximum just below the center of the region of contact and reduces with radial distance from the axis of symmetry until at the periphery of the indentation it is reduced to about 20% of the maximum value. The strain distribution is independent of indentation size, but spherical indentations scale as a/D as also does strain which is why Brinell hardness numbers depend on test parameters. Peripheral strain in spherical indentation may range from about 4% to 20%, but with spheroconical indenters based on cones with 90° included angles, peripheral strain is limited to about 14% and a/D is restricted to a maximum of 0.35. This is sufficient to observe a moderate degree of strain hardening in many materials.

The Brinell hardness number was originally defined as the mean pressure over the area of contact, with area defined as the spherically curved surface of the indentation under load enclosed by the circle delineating contact. Later, mean pressure calculated from the projected area was preferred in scientific studies as it better accords with the notion of a resolved radial stress in equilibrium with the indenting load, for example as

$$P_m = P/\pi a^2 \qquad (3)$$

where a is the radius of the contact circle.

The radius of the contact circle is traditionally measured from recovered indentations and the assumption is made that no recovery takes place in this direction on unloading. The diameter of the contact circle may also be estimated from measurements of indenter penetration, providing that the form of the indenter is sufficiently precise and proper account is taken of piling up and sinking in.

The more extensive possibilities of spherical indentation were realized by Meyer[7] who found very early

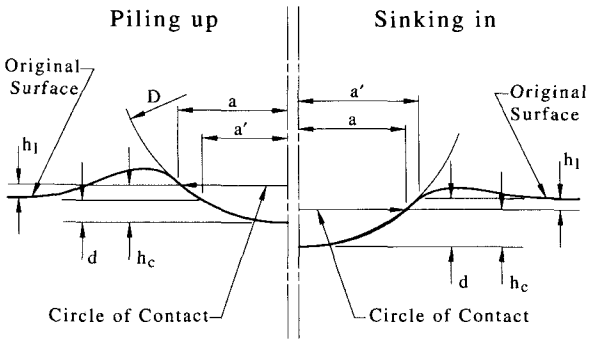

FIG. 1. Schematic representation of spherical indentation with piling up and sinking in.

that mean pressure increases with a/D according to the simple power law

$$P_m = k_1(a/D)^{1/n} \tag{4}$$

where k_1 and n are material properties.

Later O'Neill[8] showed that a substantial part of true stress versus plastic strain curves, obtained in uniaxial tension, could often be fitted by a simple power law in the form

$$\tau = k_2\lambda^{1/n} \tag{5}$$

using the same exponent, where τ is Cauchy stress and λ is plastic strain.

Combination of Eqs. (4) and (5) produces the ratio k_1/k_2, and Tabor[6] concluded from a large body of observations that

$$k_1/k_2 = \alpha\beta^{1/n} \tag{6}$$

where α and β have the substantially constant values 2.8 and 0.4 for common metals.

Combining the above expressions,

$$P_m = \alpha k_2(\beta a/D)^{1/n} \tag{7}$$

is obtained, a result that may be interpreted to show that for a material which work hardens according to a simple power law, P_m is equal to approximately 2.8 times a representative flow stress corresponding to a representative peripheral strain, given by $0.4a/D$.

The surface outside the indentation periphery is uplifted by displaced material, but the position of maximum uplift varies, being further distant for ductile materials. Material may also be drawn downward at the indentation periphery, and the contact circle may lie above or below the original surface. Norbury and Samuel[9] measured the contact circle diameter and its elevation on recovered indentations and calculated the depth of penetration h_c of the loaded indenter below the circle of contact; see Fig. 1. They found that the depth of penetration below the original surface varies as a^2 and that the ratio h_l/h_c is a material constant. The resulting numerical invariants

$$c^2 = a^2/Dd = h_c/d = 1 + h_l/d = a^2/a'^2, \tag{8}$$

in which h_c is the depth below the contact circle, and h_l is the displacement of the contact circle relative to the original surface, and a' is the radius of the circle in the plane of the original surface, are effectively independent of the index n for a wide range of materials. The elevation of the circle of contact relative to the original surface is not independent of n.

From the foregoing it is easy to see that the contact circle lies in the plane of the surface only when $c^2 = 1$, which marks the boundary between piling up and sinking in. Norbury and Samuel's[9] original data are reproduced in graphical form in Fig. 2.

Rhee and McClintock[10] showed the consistency of elastic theory with experimental data and suggested that Norbury and Samuel's data[9] could be represented by a linear, least squares fit, pinned to the value $c^2 = -0.5$ as required by elastic theory where $n = 1$. Mathews[11] extended the Hertz elastic contact solution to nonlinear viscoelastic materials including materials that work harden according to Meyer's law, and speculated that an expression of the form

$$c^2 = 1/2[(2n + 1)/2n]^{(2n-1)} - 1 \tag{9}$$

would give a better fit to Norbury and Samuel's[9] data, naturally passing through -0.5 when $n = 1$. In these investigations Norbury and Samuel's[9] data were curiously taken as h_l/d rather than h_l/h_c.

Richmond, Morrison, and Devenpeck[12] also considered an approach through nonlinear elasticity theory and obtained values of h_l/d which lay close to Norbury and Samuel's[9] data for two materials. Hill, Storåkers, and Zdunek,[13] starting from a constitutive framework outlined by Hill[14] and using nonlinear elasticity theory, determined the ratio a^2/Dd for all stages of the indentation process and verified their results by finite element methods. Meyer's law was rigorously derived from the model and the expression

$$c^2 = 5/2(2n - 1)/(4n + 1) \tag{10}$$

was proposed as a better fit to Norbury and Samuel's[9] data than Mathews's[10] expression. This expression is superimposed on Norbury and Samuel's[9] results in Fig. 2 and is a particularly good fit if the values of Meyer's index below 2.0, relating to heavily worked copper and aluminum, are omitted.

Meyer's index $(2 + 1/n)$ at the transition between piling up and sinking in was given as 16/7 which is

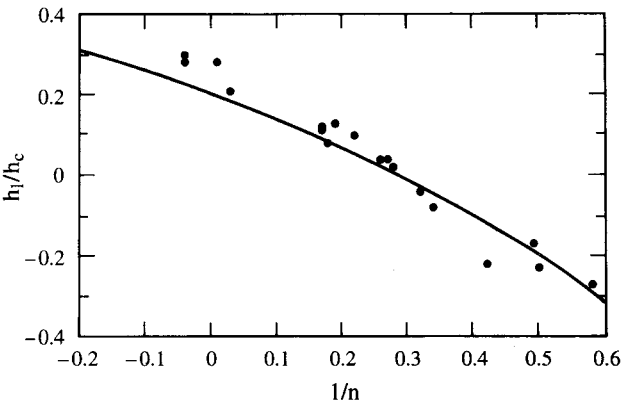

FIG. 2. Plot of Norbury and Samuel's[9] data with the equation of Hill *et al.*[13] superimposed.

indistinguishable from the value obtained by Norbury and Samuel.[9] Hill, Storåkers, and Zdunek[13] were also able to demonstrate all the observed characteristics of Brinell indentations from their model.

B. Submicrometer indentation

In the new techniques of submicrometer indentation, measurements are typically made during indentation following an increment of load. The measurements are made relative to the original surface and do not take account of the continuous change of datum which results from piling up or sinking in. Without correction such data can give only the radius a' of a circle in the plane of the original surface; see Fig. 1. However, the relationship between this radius and the radius of the contact circle is simply $a = ca'$ and correction is simple if c can be determined. Submicrometer indentation with multiple partial unloading allows values of a' to be obtained at each load step and also the value of c. Determination of c relies on rearrangement of Eq. (4) with $a = ca'$, then taking logarithms

$$\log P = \log(\pi k_1 c^{2+1/n}/D^{1/n}) + (2 + 1/n)\log a' \qquad (11)$$

A linear regression of $\log(P)$ on $\log(a')$ gives Meyer's index as the gradient, and the value of c^2 may be obtained using Eq. (9). This approach depends on the assumption of power law hardening and is applicable only when this can be demonstrated. Tabor[6] showed that when power law hardening can be assumed, yield stress is a maximum when

$$\epsilon_{\max} = 1/(n - 1) \qquad (12)$$

If the inflection of engineering tensile stress/strain curves is taken to indicate the onset of failure in work-hardening materials, this provides a useful measure of ductility.

The way is opened to these techniques by the methods discussed in the following sections.

C. General discussion of the techniques

In submicrometer indentation, load is increased incrementally and penetration is measured at each step, increments of load producing corresponding increments of elastic/plastic deformation. The separation of these data into elastic and plastic components is fundamental to the extraction of information relating to materials properties.

In the continuous load cycle method, the elastic component is obtained from measurements of recovery as the indentation is finally unloaded. The elastic and plastic components are separable only at maximum depth, and an estimate of the elastic component at intermediate steps is possible only by assuming some law of proportionality. Indentation with multiple partial unloading has been described by Field and Swain[2] and is a variant on this method. It differs by inserting a partial unloading step after each load increment. This allows the elastic component to be estimated directly at each step.

Data obtained from a test with multiple partial unloading are usually presented as plots of load versus penetration and in this respect are similar to plots of continuous load cycle data. The penetration paths followed by the two methods are usually comparable. This is illustrated in Figs. 3(a) and 3(b) which are composite plots of raw data obtained from five tests at adjacent positions on a specimen of aluminum. The rate of loading was the same for both methods—approximately 0.7 μN per second and there was a 1 s pause between the establishment of load and measurement of depth in both cases. However, the time interval between successive load steps is greater with partial unloading due to the time required to cycle the load.

The spread of penetration at maximum load apparent in the set of continuous load cycle data shown in Fig. 3(a) is typical and is usually attributed to such material variables as grain size, grain orientation, the distribution of precipitates, variation of dislocation populations, etc. Environmental variables such as temperature and vibration are also thought to play a part. Variation in the partially unloaded data shown in Fig. 3(b) is similar in magnitude but is more evenly distributed over all the data; the reason for this is not clear.

Groups of similar data are usually averaged at common loads to produce results more generally representative of the material. Figure 3(c) is a superposition of averaged data by the two methods; the close similarity is obvious. This result appears to be typical for materials that are not subject to extensive creep. Stillwell and Tabor[15] reported a small increase of plastic deformation when residual impressions in some materials were reloaded. Oliver and Pharr[16] reported a similar result when indentations in aluminum, which had been unloaded by 90%, were reloaded. No explanation of these results was given in either case, but the increase in plastic deformation was found to be more pronounced in ductile materials subject to creep. For such materials there may be a substantial time lag between the application of load and the establishment of equilibrium. The provision of a pause at each load step in the present case may have been sufficient for creep to catch up.

It is further argued that the technique of multiple partial unloading does not depend on the reversibility of elastic recovery, but rather that equilibrium is reached at the next load step as though previous unloading had not taken place, the new increment of plastic flow apparently obliterating the memory of previous unloading.

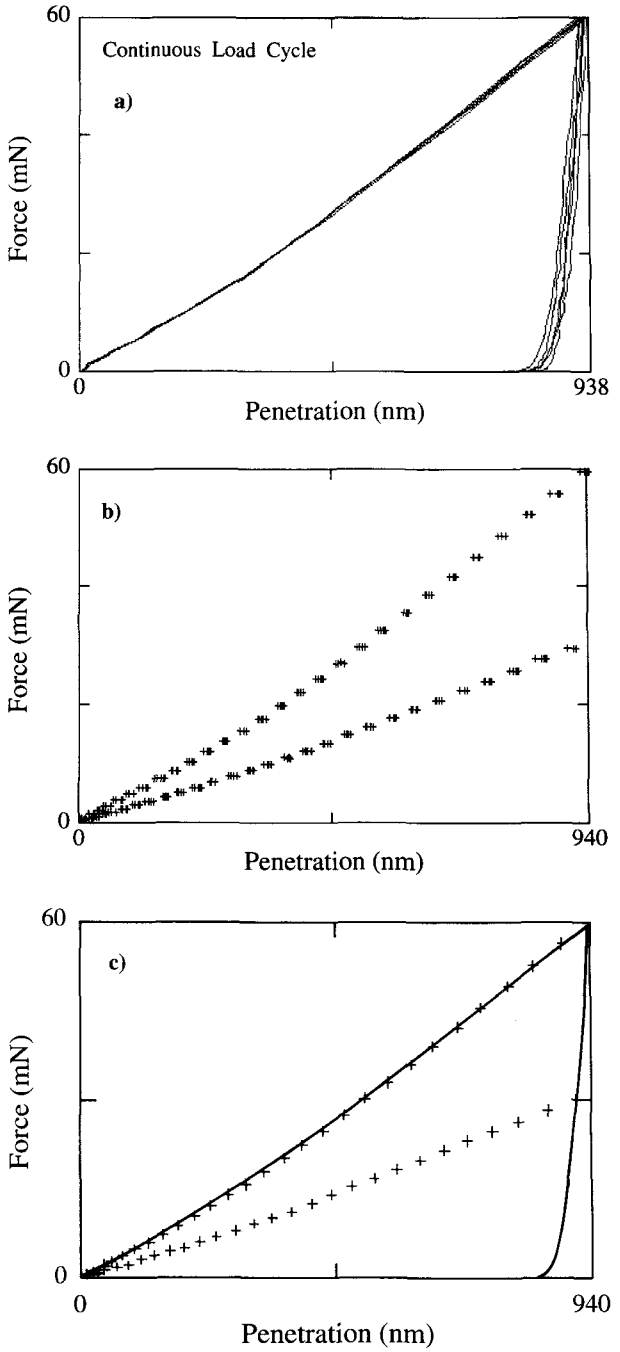

FIG. 3. Data from typical indentation sequences on aluminum: (a) continuous load cycle, (b) multiple partial unloading, and (c) superimposed averaged data.

D. The continuous load cycle method

A theoretical analysis of the relationship between load and penetration of a Vickers diamond pyramid was carried out by Loubet, Georges, and Meille,[17] and a method for interpreting the data obtained from depth-sensing instruments using a Berkovich indenter (a triangular-based pyramid with 65.3° face angles) was proposed by Doerner and Nix.[18] In these approaches it was assumed that the elastic component of penetration was similar to that produced by a frictionless, flat bottomed circular punch, pressed into a plane elastic surface.

Sneddon[19] showed that the penetration of a circular flat bottomed punch into an elastic half plane obeys the relationship

$$P = 2Eah_e/(1 - \nu^2), \tag{13}$$

where E is Young's modulus, ν is Poisson's ratio, a is the radius of the punch, and h_e is elastic penetration. The cross-sectional area of the punch was taken to be the same as the area enclosed by the perimeter of contact of the Vickers indenter, and the radius of the equivalent circular punch was calculated from this area.

The initial linearity of the relationship between P and h_e, observed in tests on some elastic/plastic materials, appeared to confirm the reasonableness of an assumption that the elastic depression of the circle of contact below the original surface could be obtained by linear extrapolation of the initial gradient, although plots of unloading data are in general curved. Applying this approach to Vickers indentations, an elastic stiffness dP/dh was postulated as the tangent to the unloading curve over its initial straight portion and was calculated as the gradient of a linear regression over the first few unloading data points. Doerner, Gardner, and Nix[20] later discussed the extension of these ideas to the investigation of thin films; however, Pharr and Oliver[21] observed that unloading data were more often curvilinear and proposed a more appropriate method of analysis.

Determination of the elastic component of spherical indentations is more secure. Johnson[5] gives the total depth of penetration of a sphere into an elastic half space as

$$h_e = (9/16)^{1/3}(P/E^*)^{2/3}\kappa^{1/3} \tag{14}$$

where κ is the mutual curvature of the contact surfaces, e.g., $1/R$ for elastic contact, where R is the radius of the indenter. Expressing stiffness as a function of the area of the contact circle, e.g., $A = \pi a^2$, it is easy to show that

$$dP/dh_e = 2E'\sqrt{(A/\pi)} \tag{15}$$

where the prime indicates $E/(1 - \nu^2)$. This gradient is the tangent to the unloading data at maximum load. The gradient at this point may be calculated by curve fitting the first few unloading data points with a suitable function [i.e., $h_e = QP^{2/3}$, Eq. (14)] and determining the inverse gradient dh_e/dP at the onset of unloading by differentiation.

Sneddon[19] also considered punches in the form of solids of revolution, such as cones, paraboloids, and

ellipsoids, and developed functions relating penetration and load. Pharr, Oliver, and Brotzen[22] examined these functions and found Eq. (15) to be a general result. In a later paper, Pharr and Oliver[21] discussed the extension of these arguments to data obtained on thin films.

The elastic penetration of a half space by a punch in the form of a solid of revolution is divided above and below the perimeter of contact, as illustrated in Fig. 4. The division depends on indenter geometry, and Oliver and Pharr[16] showed that the elastic depression of the circle of contact below its unloaded position is given by

$$h_1 = qP_{\max}dh_e/dP \tag{16}$$

where q is exactly 0.75 for a paraboloid and may be taken as 0.75 for a Berkovich indenter with reasonable accuracy.

Starting from Eq. (14) it is easy to show that for a spherical indentation

$$dP/dh_e = 1.5P_{\max}/h_e \tag{17}$$

The penetration of a rigid sphere into an elastic half space is equally divided above and below the circle of contact and consequently the elastic depression of the circle of contact may be calculated using

$$h_1 = 0.75P_{\max}dh_e/dP \tag{18}$$

Thus q in Eq. (16) may also be taken as 0.75 for a sphere.

Penetration below the circle in the plane of the original surface h_b may be calculated from the measured penetration h_m by subtraction, e.g.,

$$h_b = h_m - h_1 \tag{19}$$

The radius a' of this circle may be calculated from h_b using the spherical radius of the indenter in

$$a' = \sqrt{(2Rh_b - h_b{}^2)} \tag{20}$$

However, no information is available from which the radius of the true circle of contact may be calculated, consequently the best available estimate, a' must be used. It is also easy to show from Eq. (14) that E^* may be estimated as

$$E^* = 0.75P_{\max}/ah_e \tag{21}$$

Using a' as an estimate for a, an error in E^* arises that is proportional to the unknown value of c. The projected area of the contact circle estimated as $A = \pi a'^2$ and used to calculate hardness as

$$H = P/A \tag{22}$$

produces an error in H proportional to $1/c^2$.

E. The multiple partial unloading method

Tabor[6] showed that unloading a spherical indentation from beyond the onset of full plastic flow leaves a spherical impression in the surface with a spherical radius larger than that of the indenter. Assuming complete reversibility, the elastic component of a partially unloaded indentation is similar to the elastic depression produced by loading a suitably dimensioned preformed spherical cavity to the same load.

Stillwell and Tabor[15] showed that the elastic deformation produced by loading a spherical indenter into a preformed spherical cavity may be calculated from an expression similar to Eq. (14), but with κ redefined as

$$\kappa = 1/R - 1/R_1 \tag{23}$$

R remains the indenter radius, but R_1 is the radius of the preformed cavity. This is illustrated diagrammatically in Fig. 5.

Field and Swain[2] showed that given a total measured penetration h_t at some load P_t and a partially recovered

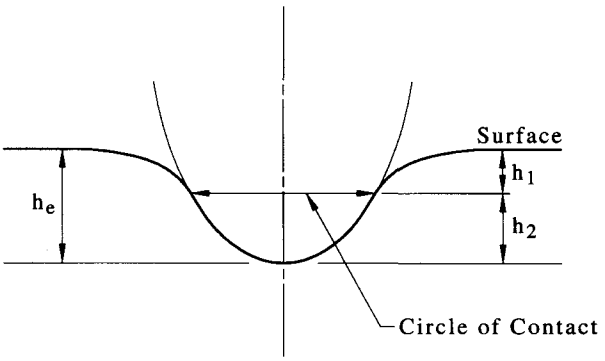

FIG. 4. Schematic geometry of elastic contact between an indenter in the form of a solid of revolution and an elastic half space.

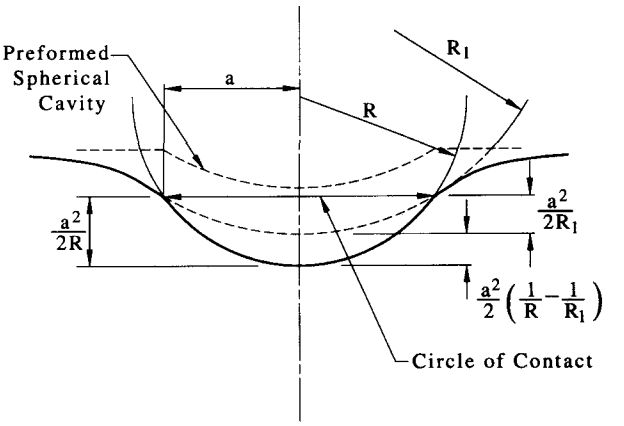

FIG. 5. Schematic geometry of preformed spherical cavity loaded with a spherical indenter.

depth h_s at a reduced load P_s, the depth of the residual impression relative to the original surface on fully unloading may be calculated from

$$h_r = (rh_s - h_t)/(r - 1) \quad (24)$$

using

$$h_t/h_s = (P_t/P_s)^{2/3} \quad (25)$$

and Eq. (14) to obtain

$$r = (P_t/P_s)^{2/3} \quad (26)$$

Then the elastic component of indentation at each load step may be calculated using

$$h_e = h_t - h_r \quad (27)$$

and the unloading stiffness at the onset of unloading from each increment of load using $dP/dh_e = 3P/2h_e$.

The depth of penetration below the circle in the plane of the surface at each step may be calculated from

$$h_b = h_r + h_e/2 \quad (28)$$

and the radius a' from Eq. (20).

A regression of $\log(P)$ on $\log(a')$ then gives Meyer's index $(2 + 1/n)$, allowing c to be calculated from $1/n$ using Eq. (10). The radius of the true contact circle at each step may then be calculated using $a = ca'$ and the depth below the circle of contact using $h_c = c^2 h_b$, or

$$h_c = R - \sqrt{(R^2 - a^2)} \quad (29)$$

Values for the composite modulus E^* may be determined at each step using Eq. (21) or alternatively E^* may be corrected subsequently by multiplication by c. Hardness may be calculated using Eq. (22) with the corrected value of a or subsequently corrected by division by c^2.

F. Discussion of assumptions

In deriving the above expressions a tacit assumption of perfect indenter form is made. For example, in the derivation of Eq. (24) it is assumed that the effective spherical radius of the indenter R_t at penetration h_t is the same as the effective spherical radius of the indenter R_s at penetration h_s. Similarly we have assumed that the indenter spherical radius is the same at depth h_b as it is at depth h_c. This is often not quite true since the generation of perfectly formed solids of revolution in diamond is still not possible. An error may be introduced into h_r calculated from Eq. (24) if the spherical radius ratio R_s/R_t is significantly different from unity. However, the elastic recovery $(h_t - h_s)$ is not usually large compared with the total penetration h_t for metallic materials, and the change in effective spherical radius of the indenter over this distance is usually small. The calculation of r, in Eq. (26), is reasonably robust and this error has been ignored. Further errors in h_r may arise from incomplete correction for the elastic compliance of the instrument structure and incomplete knowledge of the position of the indenter on contact with the surface; the methods of correction for these will be discussed later. It has also been assumed that Norbury and Samuel's[9] and Meyer's[7] results can be applied to indentation on a very small scale. It is well known that some materials do not show classical power law hardening at small strains and for these materials it may be necessary to apply a lower limit to the indentation radius included in a regression of $\log(P)$ on $\log(a')$.

III. EXPERIMENTAL

Experimental methods

Two steel specimens were used to illustrate the determination of hardness and modulus as functions of load: one with a nominal hardness of 200 HV and the other with a nominal hardness of 500 HV. A pure aluminum specimen with a nominal hardness of 100 HV was also used. The possibility of determining Meyer's index from these results was examined, and the consequences of anomalous strain hardening are discussed.

The two steel specimens were commercial microhardness blocks with fine-grained microstructure and finely dispersed precipitates typical of heat-treated carbon steel. The aluminum specimen was annealed and progressively polished to a high finish with care taken to minimize work hardening of the surface.

Experiments were carried out using a UMIS 2000 submicrometer indentation system (UMIS is the registered name of an instrument developed and manufactured by CSIRO Division of Applied Physics, Lindfield, Australia) with multiple partial unloading, and each specimen was the subject of several experiments. Each experiment consisted of producing five indentations in a line separated by a distance sufficient to avoid interaction. The region of the specimen chosen for each run was as free as possible from visible defects when observed under a high power microscope. For each run the instrument was set up and allowed to stand until the in-built stability sensor showed no drift, after which the five indentations were produced automatically. For the steel specimens 100 data points were used and in the aluminum 30 data points were used. The lower number is sufficient for normal material evaluation, but the larger number gives a finer spacing of data points and is more suitable for evaluating the determination of Meyer's index. In all cases multiple partial unloading was used with unloading to 50%.

Two spheroconical indenters were used both based on 90° cones, one with a tip radius of 10 μm and the

other with a tip radius of 5 μm. The form of the indenters was examined by scanning electron microscopy. Figures 6(a) and 6(b) are photomicrographs of typical axial sections. The spherocone with a 10 μm tip radius was well formed and well blended to the cone, but the 5 μm tip radius of the other spherocone although well formed was poorly blended to the cone, giving a sharp change in geometry at about 500 nm depth. Photomicrographs of both spherocones were also examined using a technique in which the photomicrograph profiles were digitized. They were both found to depart slightly from perfect spherical form at the tip, but only the poorly blended 5 μm spherocone showed significant departures from ideal form. Although the value of the local spherical radius may influence results where the nominal value was used, it is very difficult to characterize the shape of imperfect spheres and this has not been attempted. The actual best fitting spherical radius was found to be 8.5 μm for the nominally 10 μm indenter to a depth of 2.5 μm and 5 μm for the nominally 5 μm indenter to a depth of 0.5 μm. Although penetration was allowed to pass the geometry change with the 5 μm indenter, caution has been exercised in analyzing these results. Both indenters were used on all three materials, but only selected results are presented.

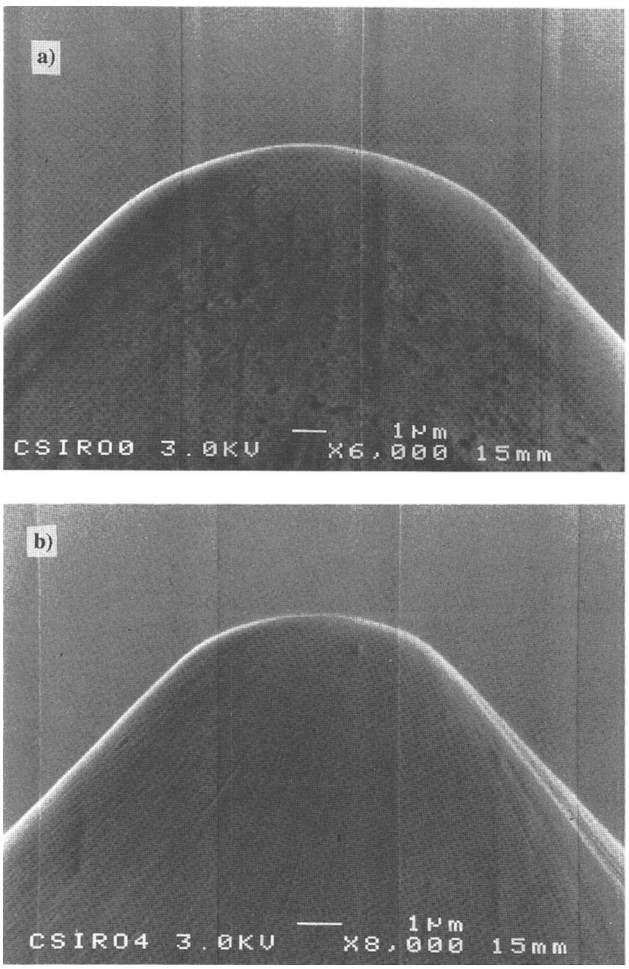

FIG. 6. SEM photographs of indenter profiles for (a) 10 μm radius and (b) 5 μm radius.

IV. RESULTS

Figure 7 is a photomicrograph of a group of indentations in the 500 HV steel specimen using the 10 μm indenter. This is typical of all the results obtained.

A. The steel specimens

Figure 8(a) is a composite plot of the data obtained with the 5 μm indenter on the 500 HV hardness steel specimen. This is also typical of steel; plots of results on materials with similar values of H/E are usually similar, differences becoming apparent only on analysis. The spread of data at the maximum load is also typical and may be attributed to variations in material structure. The effects of imperfect geometry beyond a combined elastic/plastic penetration of about 600 nm are also evident. The data for each group of similar indentations were generally consistent, and the data for each group were averaged point by point; Fig. 8(b) is the average of the data shown in Fig. 8(a).

Analysis commenced with correction for instrument compliance determined using the method recommended by the instrument maker. Since all depth measurements are made relative to a datum established under a small contact load, a correction must also be made for the penetration this produces. The correction was estimated by performing a linear regression of h_t on P or $P^{2/3}$ for the first five data points, the exponent depending on whether the initial deformation is considered to be elastic or elastic/plastic, the choice in practice depending on which gives the higher correlation.

The residual penetration and elastic component were then calculated at each load step using the methods

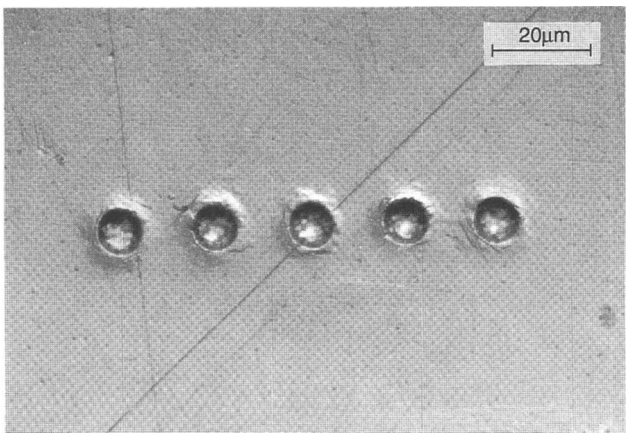

FIG. 7. Photomicrograph of a group of indentations: 20 μm indenter in the nominally 500 HV steel hardness block.

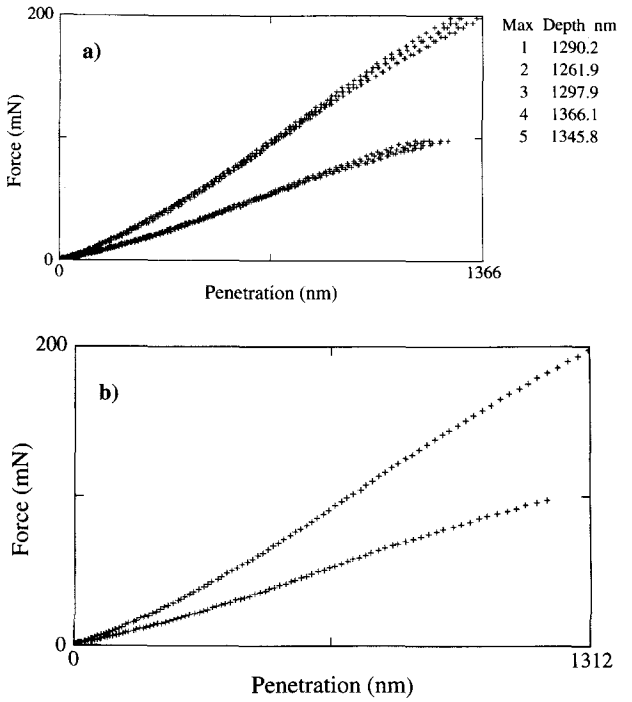

FIG. 8. Data from the indentation of the nominally 500 HV steel hardness block using the nominally 5 μm indenter: (a) raw data and (b) averaged data.

previously described. These were then used to determine the radius a' of the circle in the plane of the original surface and the depth of penetration h_b below this circle. A regression of $\log(P)$ on $\log(a')$ was then performed to examine the assumption of power law hardening. Power law hardening was assumed to be operating if $\log(P)$ was highly correlated with $\log(a')$ and the gradient was between 2.0 and 2.6 as suggested by Tabor.[6] Typical results were as follows: 200 HV steel: 10 μm indenter, correlation coefficient $r = 0.998$, gradient = 2.156, and $c = 1.053$; 500 HV steel: 5 μm indenter, correlation coefficient $r = 0.9997$, gradient = 2.456, and $c = 0.931$.

Figure 9 is a plot of $\log(P)$ versus $\log(a')$ for the 500 HV steel specimen; other results were similar. For both materials the correlation is good, the 500 HV material being generally a little better. The values of c indicate sinking in for the 200 HV steel and piling up for the 500 HV steel.

The composite modulus for the 500 HV specimen, calculated using Eq. (21), is shown in Fig. 10(a) and its hardness, calculated from Eq. (22) in Fig. 10(b). The modulus for the two steel specimens was very similar and is not shown for the 200 HV specimen, but its hardness is shown in Fig. 10(b). Note the plateau-like behavior for the hardness (or mean contact pressure) versus depth for penetrations greater than 600 nm resulting from indenter geometry. The modulus values are determined from the elastic component of indentation and are

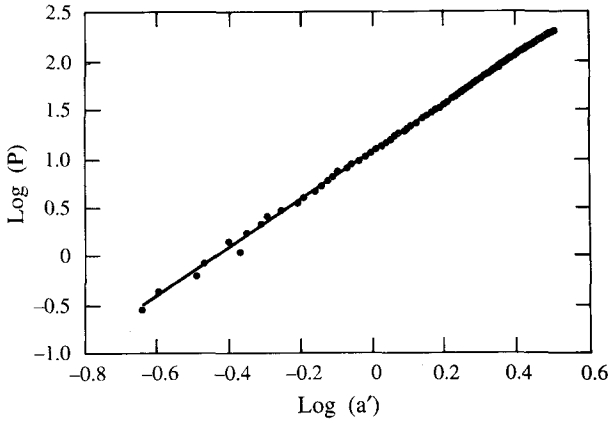

FIG. 9. Log(P) (load) versus log(a') for the nominally 500 HV steel specimen.

somewhat noisy, but the values are close to the expected values of 198 GPa. These are composite modulus values and include the compliance of the indenter. Young's modulus and Poisson's ratio for diamond are variously quoted in the literature (see Field[23]). The values chosen were $E_i = 1000$ GPa and $\nu_i = 0.1$, respectively.

The hardness values are quite different. The 500 HV specimen shows an initial steep rise that is thought

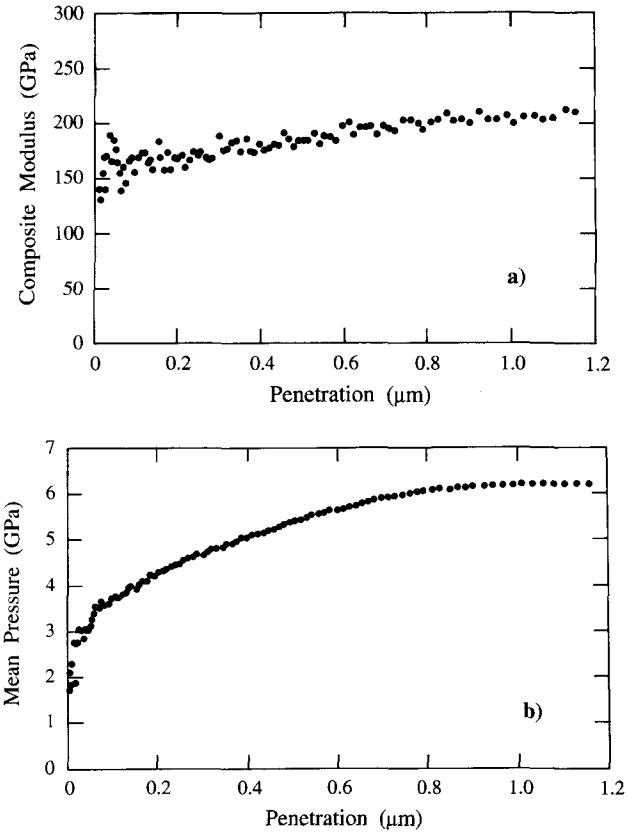

FIG. 10. 500 HV steel specimen: (a) composite modulus and (b) hardness or contact pressure.

to reflect the transition from elastic to plastic flow conditions. Then hardness rises exponentially to a value a little over 6 GPa. This is a little higher than the expected value of 5.5 GPa. The hardness of the 200 HV specimen after an initial sharp rise falls to about 1.6 GPa and then climbs exponentially to about 2.2 GPa, which is very close to the expected value. The behavior of the hardness plots at very small penetration is strongly affected by departure of the indenter from true spherical geometry and should be interpreted cautiously.

Figure 11 is a plot of representative stress (mean pressure) versus representative strain ($\epsilon_r = 0.2ca'/R$) for the 500 HV steel specimen.

B. The aluminum specimen

Figure 12(a) is a composite plot of the data obtained with the 10 μm indenter on the aluminum specimen. This is typical of ductile materials and differs from the steel results in that the elastic component is relatively much smaller. The averaged data are shown in Fig. 12(b).

Again analysis commenced with correction for instrument compliance and determination of a contact correction. The residual penetration and elastic component were then calculated at each load step and used to determine the radius a' of the circle in the plane of the original surface and the depth of penetration h_b. A regression of $\log(P)$ on $\log(a')$ was then performed to examine the assumption of power law hardening with the result: correlation coefficient $r = 0.9991$ and gradient $= 1.882$.

Figure 13 is a plot of $\log(P)$ versus $\log(a')$. Since the gradient is less than 2, it was concluded that power law hardening may not be an appropriate model although the correlation is good. This suggests there may be an oxide or work-hardened layer on the aluminum that raises the initial yield point and results in the observed strain softening behavior. The composite modulus was calculated using Eq. (21) with the circle of contact radius

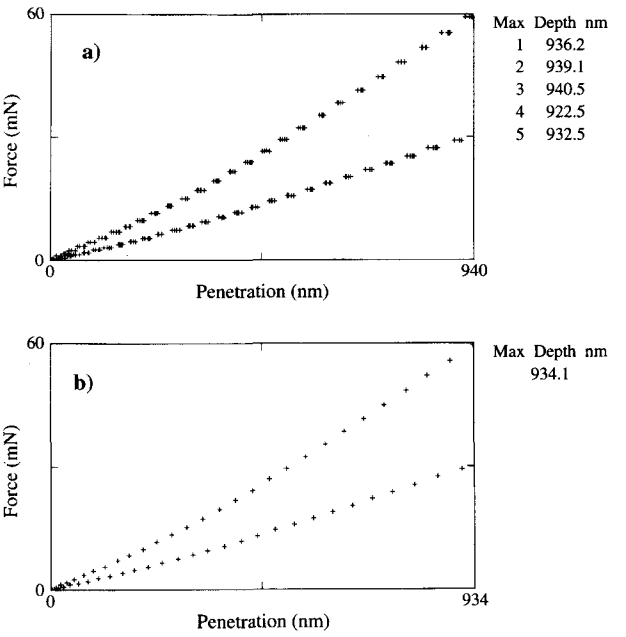

FIG. 12. Data from the indentation of the aluminum specimen using the nominally 10 μm indenter: (a) raw data and (b) averaged data.

estimated by a' and is shown in Fig. 14(a), and hardness, calculated from Eq. (22) on the same basis, is shown in Fig. 14(b). The modulus initially falls to about the value expected, 71 GPa, and then rises steadily to 150 GPa. This high value is not typical of aluminum and indicates some other influences that will be discussed later. The hardness, after an initial sharp rise, falls to about 0.9 GPa and then climbs exponentially to about 1.1 GPa, which is reasonable.

V. DISCUSSION

Not all materials are appropriate for the determination of Meyer's index by the methods outlined. However, a linear correlation between $\log(P)$ versus $\log(a')$ may be found when some influence in addition to power law

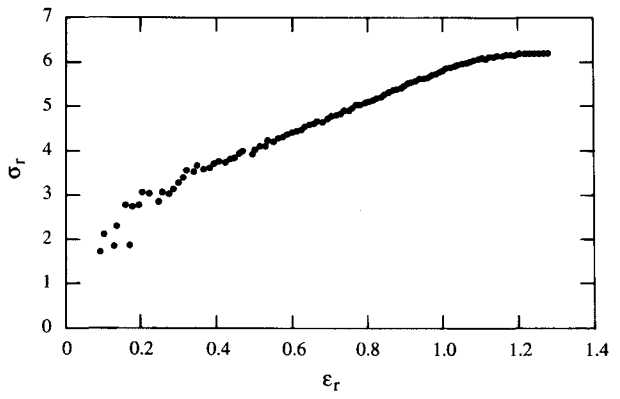

FIG. 11. Representative stress/strain plot for the 500 HV steel specimen.

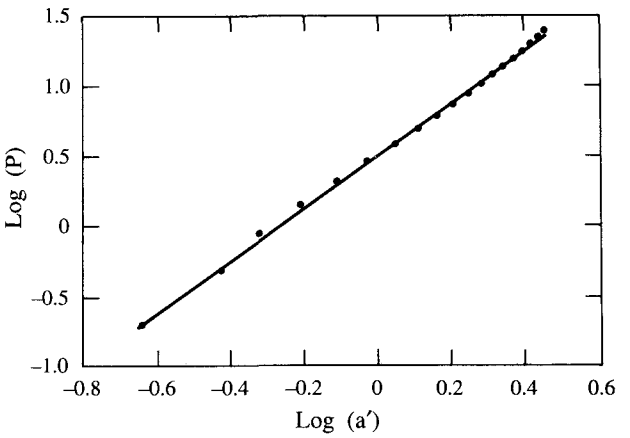

FIG. 13. Log(P) (load) versus log(a') for the aluminum specimen.

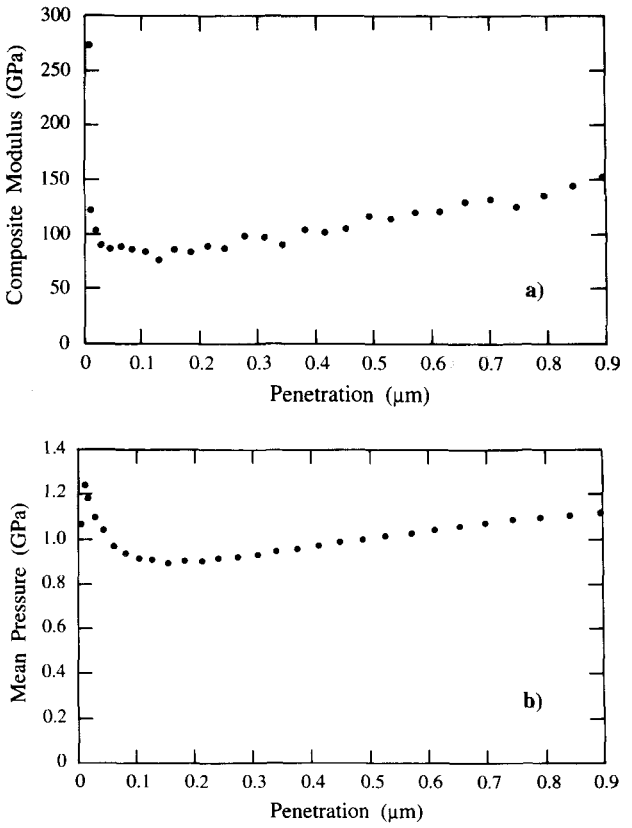

FIG. 14. Aluminum specimen: (a) composite modulus and (b) hardness.

hardening is operating. There are a number of situations in which the assumption of power law hardening may not be appropriate, for example, the initial anomalous behavior of steel at the onset of plastic strain. Aluminum oxidizes readily and is easily work hardened by polishing, leaving a hard and possibly brittle skin. The strength of this skin is higher than the underlying material and supports a disproportionate amount of the load during indentation; also, its elastic modulus may be much higher than the underlying material. Initial elastic indentation will reflect the modulus of the skin until a crack forms, allowing the full load to be applied to the underlying material. A part of the load may continue to be supported by this strong skin with successive fracture events as load is increased. At any quiescent point residual penetration may be less than for the bulk material, invalidating the methods described. Consequently, indentation through a hard surface layer or to within a small distance of a hard substrate may not be amenable to analysis by this method. However, with these reservations in mind partial analysis of such data may still be useful.

A. Indenter geometry

Among the many sources of uncertainty that arise in submicrometer indentation, the one least well accounted for is indenter geometry. Indenters are three-dimensional objects and are ideally described in terms of deviations from an ideal shape at many points on a three-dimensional map. Methods for calibrating indenters in this way have not been developed although techniques for three-dimensional modeling using the atomic force microscope (AFM) and scanning electron microscope (SEM) are under examination. At present a less precise method must be used based on such collective measures as cross-sectional area, effective contact circle radius, or effective spherical radius, each expressed as a function of distance from the tip.

A method for determining the cross-sectional area of Berkovich diamond pyramids was described by Doerner and Nix.[18] This involves the production of replicas from indentations in a standard material followed by calculation of the projected area from a TEM image. Repeated at different loads the cross-sectional area of the indenter is determined as a function of depth. To obtain a reasonable picture of indenter form, a large number of indentations must be analyzed and, although a similar approach is applicable to spherical indenters, it is much too expensive for routine use. A simpler method was developed as part of the application software for the UMIS instrument. In this method a comparison is made between actual penetration depths in a standard material and those expected for a perfectly formed indenter. Differences are interpreted as being due to errors of indenter form, and a correction look-up table is automatically produced.

Oliver and Pharr[16] also described a method that makes use of the constancy of elastic modulus and demonstrated it using indentations of increasing size in aluminum. They then used an iterative method to obtain a polynomial representing indenter cross-sectional area as a function of depth with instrument compliance as a by-product.

These methods may also be applicable to spherical indenters, but departures from spherical geometry are more complicated than are those arising with pyramids. In the present work the nominal radii of the indenters have been used and at small penetrations some error undoubtedly arose from this.

B. General comments

Indentation with spherical indenters offers many opportunities for examining the indentation behavior of very small volumes of material. It is clear, however, that present understanding is insufficient to extract all the information present in the data. Hardness is representative of yield stress but on any scale it is a confusing mixture of responses and is affected by such variables as grain size, anisotropy, impurities, precipitates, and the combined influence of these on the mobility of dis-

locations. As a function of depth, hardness is represented on a changing scale and represents a changing picture of these interactions. When a surface has been deliberately modified by heat treatment, diffusion, implantation, or coating with a foreign species, yield stress may vary with depth and this will further cloud the picture. However, it is important to be able to monitor such changes even though the data may not be fully understood. The methods outlined in this paper provide that opportunity, and the values produced are similar to those expected when straightforward materials are tested. The techniques described cannot give unambiguous values of Young's modulus or Poisson's ratio, but again it may be possible to monitor the changes produced by surface modification. A plot of composite modulus as a function of penetration can also indicate the influence of a near surface substrate material.

It may also be possible to determine the radius of the circle of contact from the elastic component of indentation by assuming values of Young's modulus and Poisson's ratio for the material. This should not be overlooked since it allows hardness to be estimated independently of piling up or sinking in and non-power-law strain hardening or softening to be examined without performing a regression of $\log(P)$ on $\log(a')$. The need to assume Young's modulus and Poisson's ratio is often not unreasonable since both are well known for many materials and are usually unaffected by working. However, the results obtained by multiple partial unloading are somewhat noisy.

The distribution of stress under a spherical indenter, indenting a homogeneous material within the Meyer regime, is constant regardless of indentation size, and its magnitude is well represented by mean pressure. Also, as suggested by Tabor[6] and subsequently shown by Hill, Storåkers, and Zdunek,[13] the strain contour at 0.2 ϵ_{max} approaches the surface at the indentation periphery regardless of indentation size. Consequently, representative stress/strain curves are indicative of stress/strain curves normally obtained in uniaxial tension or compression. Since these are virtually impossible to obtain any other way for small volumes of material, this approach is also of value.

VI. CONCLUSIONS

The methods described provide a means of obtaining otherwise unavailable information about very small volumes of material and for dealing with the problem of piling up and sinking in. In particular the method of multiple partial unloading allows more information to be extracted than can be obtained from continuous load cycles. Both methods have the advantage of rapid automatic data acquisition and good reproducibility, and a full analysis is possible from a single indentation, repetition being required only to reduce noise. Now that the empirical results of Tabor,[6] Meyer,[7] O'Neill,[8] and Norbury and Samuel[9] have been placed on a firm foundation by Hill, Storåkers, and Zdunek,[13] the basic models are relatively simple. However, the models do not cover all indentation situations and the results must be interpreted carefully.

REFERENCES

1. J. A. Brinell, Congress Int. des Methods d'Essai des Mat. de Construction, Paris **2**, 83 (1901).
2. J. S. Field and M. V. Swain, J. Mater. Res. **8**, 297 (1993).
3. H. A. Francis, Trans. ASME (Series H) **9**, 272 (1976).
4. H. Hertz, J. reine u. angew. Math (Crelle) **92**, 156 (1882).
5. K. L. Johnson, *Contact Mechanics* (Cambridge University Press, Cambridge, UK, 1985).
6. D. Tabor, *Hardness of Solids* (Oxford University Press, Oxford, UK, 1951).
7. E. Meyer, Z. Ver Deutsch Ing. **52**, 645 (1908).
8. H. O'Neill, Proc. Inst. Mech. Eng. **151**, 116 (1944).
9. A. L. Norbury and T. Samuel, J. Iron Steel Inst. **117**, 673 (1928).
10. S. S. Rhee and F. M. McClintock, Proc. 4th U.S. Natl. Cong. Appl. Mech., 1007 (1962).
11. J. R. Mathews, Acta Metall. **28**, 311 (1980).
12. O. Richmond, H. L. Morrison, and M. L. Devenpeck, Int. J. Mech. Sci. **16**, 75 (1974).
13. R. Hill, B. Storåkers, and A. B. Zdunek, Proc. R. Soc. London **A423**, 301 (1989).
14. R. Hill, J. Mech. Phys. Solids **35**, 565 (1987).
15. N. A. Stillwell and D. Tabor, Phys. Soc. Proc. **78**, 169 (1961).
16. W. C. Oliver and G. M. Pharr, J. Mater. Res. **7**, 1564 (1992).
17. J. L. Loubet, J. M. Georges, and G. Meille, in *Microindentation Techniques in Materials Science and Engineering*, edited by P. J. Blau and B. R. Lawn (ASTM Special Technical Publication, Philiadelphia, 1985), p. 72.
18. M. F. Doerner and W. D. Nix, J. Mater. Res. **1**, 601 (1986).
19. I. N. Sneddon, Int. J. Eng. Sci. **3**, 47 (1965).
20. M. F. Doerner, D. S. Gardner, and W. D. Nix, J. Mater. Res. **1**, 845 (1986).
21. G. M. Pharr and W. C. Oliver, MRS Bull. (July 1992).
22. G. M. Pharr, W. C. Oliver, and F. R. Brotzen, J. Mater. Res. **7**, 613 (1992).
23. *The Properties of Diamond*, edited by J. E. Field (Academic Press, London, 1979).